Chin. Phys. Lett. **39**, 028202 (2022)

Electrochemical Role of Transition Metals in Sn–Fe Alloy Revealed by Operando Magnetometry

Le-Qing Zhang(张乐清)[1], Qing-Tao Xia(夏清涛)[1], Zhao-Hui Li(李召辉)[1], Yuan-Yuan Han(韩媛媛)[1], Xi-Xiang Xu(徐熙祥)[1], Xin-Long Zhao(赵新龙)[1], Xia Wang(王霞)[1], Yuan-Yuan Pan(潘圆圆)[1], Hong-Sen Li(李洪森)[1], and Qiang Li(李强)[1,2*]

[1]*College of Physics, Qingdao University, Qingdao 266071, China*
[2]*Weihai Innovation Institute, Qingdao University, Weihai 264200, China*

(Received 5 November 2021; accepted 23 December 2021; published online 29 January 2022)

As promising materials, alloy-type anode materials have been intensively investigated in both academia and industry. To release huge volume expansion during alloying/dealloying process, they are usually doped with transition metals. However, the electrochemical role of transition metals has not been fully understood. Here, pure Sn_3Fe films were deposited by sputtering, and the electrochemical mechanism was systematically investigated by operando magnetometry. We confirmed that Fe particles liberated by Li insertion recombine partially with Sn during the delithiation, while the stepwise increase in magnetization with the cycles demonstrates growth of Fe nanoparticles. In addition, we also found an unconventional increase of magnetization in the charging process, which can be attributed to the space charge storage at the interface of Fe/Li_xSn. These critical findings pave the way for the mechanism understanding and development of high-performance Sn based alloy electrode materials.

DOI: 10.1088/0256-307X/39/2/028202

As the great supports for smart grids, electric vehicles, and micro/nanodevices, lithium-ion batteries (LIBs) have become cornerstone of energy storage technology.[1–7] The ever-growing technological demand for higher-energy systems keeps catalyzing the exploration of higher-capacity LIB electrode materials.[8–11] Reacting with Li via alloying reaction, tin has long been considered as a promising alternative to graphite anodes due to its high specific capacities.[11,12] However, substantial volumetric expansion of 257% on the complete Li insertion in Sn causes fragmentation/loss of the particles, thus leading to a rapid deterioration in the cycling.[11,13–17] In order to mitigate this issue, transition metals (Fe, Co, Ni, etc.) have been usually introduced as a buffer matrix to relieve the volume expansion.[18–22] Early successful commercialization of Sn–Co alloy electrodes was released in the SONY Nexelion battery in 2004.[23] So far, despite the great progress made in Sn-based alloys for LIBs, the role of transition metals in electrochemical reaction upon lithiation/delithiation is still unclear and controversial.[24–26]

Among the various Sn-based anodes, being earth-abundant, cost-effective and eco-friendly, Sn–Fe alloys have aroused intense interest and have been extensively investigated in recent years.[27–29] However, it is still a matter of debate whether Fe, as an inactive center, can be alloyed reversibly with Sn during cycling. By using *in situ* x-ray diffraction and *in situ* Mössbauer spectroscopy, Dahn *et al.* found that the iron particles formed during discharge were not completely inactive and re-alloyed with Sn following charged.[30] By contrast, Nwokeke *et al.* proposed that the morphology of iron nanoparticles produced while embedded lithium was maintained in the subsequent cycles being completely inert.[31] Nevertheless, Whittingham *et al.* reported that some Fe particles remained after the first cycle of charging without recombining with Sn revealed by a combination of x-ray diffraction and x-ray absorption spectroscopy.[32] Therefore, it is crucial to unravel the electrochemical mechanism during alloying reaction, especially the role of transition metals.[33–35]

Due to the high sensitivity to magnetic materials, magnetometry provides a powerful tool to gain insights into the electrochemical mechanism from the perspective of the charge and magnetic interaction.[36–38] To data, magneto-electrochemistry is now understood being common, suggesting promising new concepts of uncovering electrochemical mechanism through magnetic theory and techniques.[39] In this work, we prepared high-pure Sn–Fe alloys without binders and conductive additives via magnetron sputtering deposition, guaranteeing all of the magnetic variations are mainly due to iron element.[8,40] A magnetometry coupled with electrochemistry was performed to monitor, *in situ*, the time evolution of voltage and magnetization in Sn–Fe/Li cells. The sig-

*Corresponding author. Email: liqiang@qdu.edu.cn
© 2022 Chinese Physical Society and IOP Publishing Ltd

nificantly higher magnetization at 2 V compared to the original samples indicates that the Fe particles are partially re-alloyed with Sn as the removal of Li, while the rest of Fe remains metallic elemental state during cycling. Further magnetometry proved that the stepwise increase in magnetization with the cycles is caused by the increase in the size of iron particles. Excitingly, abnormal magnetic response during charging process reveals the phenomenon of space charge storage in alloy materials, which provides extra capacity for batteries. These critical findings help open the way for better understanding the role of transition metals in electrochemical alloying/dealloying processes and the rational design of high-performance electrode materials for LIBs.

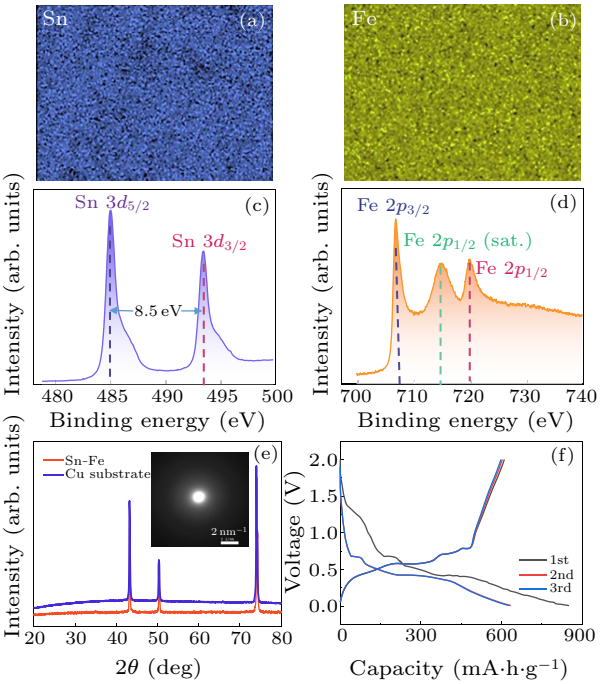

Fig. 1. Structural and compositional characterization of the initial sample, and the basic electrochemical properties for the Sn–Fe alloy anode in LIBs. The EDX element mapping diagram of the Sn element (a) and Fe element (b), marked blue and yellow, respectively. The XPS spectrum of the Sn $3d$ (c) and Fe $2p$ (d) in Sn–Fe alloy film. (e) XRD pattern of the Sn–Fe and Cu substrate (SAED image of Sn–Fe in the inset). (f) Galvanostatic charge-discharge curves of the initial three cycles at 100 mA·g^{-1}.

Pure Sn–Fe alloys were prepared by magnetron co-evaporation from tin and iron targets (purity 99.99%) with an Ar gas pressure of 22.5 mTorr at room temperature. The deposition powers applied to the Fe and Sn targets were 10 W and 10 W, respectively. During the sputtering process, the substrate (copper foil) was rotated to ensure uniformity of Sn–Fe alloys. The mass was obtained by measuring the difference of substrate before and after deposition via electrobalance (METTLER TOLEDO). The thickness of the nanocomposite film is approximately as determined by atomic force microscope (AFM, Park systems XE7). Predictably, TEM energy dispersive x-ray spectroscopy (EDX) mapping images [Figs. 1(a) and 1(b)] provided clear evidence of high homogeneity of Sn and Fe elements in the films. Furthermore, the EDX spectrum in Fig. S1 of the Supplementary Material shows the Sn and Fe atomic ratios of 77% and 23%, respectively, thus the electrodes are approximated as Sn_3Fe. Figures 1(c) and 1(d) show the high-resolution XPS spectra of Sn $3d$ and Fe $2p$ collected from the as-growing samples. In Fig. 1(c), the binding energy difference between Sn $3d_{5/2}$ (484.9 eV) and Sn $3d_{3/2}$ (493.9 eV) is 8.5 eV,[41] which excludes the presence of tin oxides. The two characteristic peaks centered at 706.7 and 719.8 eV correspond well with the $2p_{3/2}$ and $2p_{1/2}$ peaks of metallic Fe [Fig. 1(d)].[42,43] The XRD patterns in Fig. 1(e) show that there is no diffraction peak other than those of the Cu substrate, which indicates that the thin film is in the nanocrystalline or amorphous state. TEM selective area electron diffraction (SAED) diagram shown in the inset exhibits a diffuse ring, which also shows that the sample is in the amorphous state. According to previous reports,[44] amorphous phase is favorable to release the volume expansion of the tin-based anode, which ensures excellent electrochemical performance in the cycle life.

Sn–Fe alloys were assembled into LIBs to serve as working electrodes, with $LiPF_6$ (1 M, in 1 : 1 w/w ethylene carbonate/dimethyl carbonate) utilized as the electrolyte. Then, electrochemical properties of Sn_3Fe electrode were evaluated through charge/discharge curves at constant current density of 100 mA·g^{-1} as shown in Fig. 1(f). The second and third charge/discharge curves almost overlap, yielding a reversible capacity of 628 mA·h·g^{-1}. Figure S2 in the Supplementary Material shows that a capacity of 605 mA·h·g^{-1} was delivered by Sn_3Fe LIBs in the tenth cycle, indicating the good cycling stability. Distinctly, Sn–Fe anodes not only have a better cycle stability through reducing the volume expansion, but also have a higher capacity performance than pure Sn anodes.

To understand the electrochemical mechanism, coupling operando magnetometry with cyclic voltammetry (CV) of the Sn_3Fe LIBs measurement was performed in Fig. 2. As shown in Fig. 2(a), the cathodic peaks from 0.68 to 0.18 V correspond to the progressive formation of Li_xSn ($0 \le x \le 4.4$) alloys, which also means the dealloying process of Fe from Sn_3Fe. Accordingly, the anodic peaks from 0.4 to 0.9 V are related to the stepwise decomposition of Li_xSn with the lithium extraction process, which is consistent with the previous reports.[14] The irreversible capacity loss in the first 1–1.5 V discharge results from the generation of the solid electrolyte interface.[22,32] The temporal evolutions in the magnetization of Sn_3Fe follow

the periodicity of the voltage under the condition of constant magnetic field 1 T and 300 K [Fig. 2(b)]. The magnetization values given in emu·g^{-1} are defined per unit weight of active materials (Sn_3Fe). As revealed by Fig. S3 in the Supplementary Material, continuously sampling through magnetization on a cell assembled with or without active materials, the tiny constant value of the background signal during cycling makes no effect in variation of the magnetization. This means that no obstacle existed in further exploring the electrochemical role of transition metals in alloys. The linear magnetic background signals from the other cell assembly components, such as the Li metal, electrolyte, separator and copper foil, is deducted from the total magnetic moment in Fig. 2(b). The initial low magnetization indicates that the prepared sample is mainly in the form of alloy. Before reaching 0.31 V upon lithiation, the magnetization remains stationary. Until the discharge voltage is below 0.31 V, there is a sharp increase in magnetization, which is related to the dealloying of Fe from Sn_3Fe. In the subsequent charging process, the voltage range of 0.67–1.01 V corresponds to a significant decrease in magnetization, indicating the re-formation of Sn–Fe alloy. However, the higher magnetization at 2 V compared to that of the initial film proves that a part of Fe remains as metallic element state. The fact that Fe formed by the first lithiation is partially reversible upon delithiation is revealed, that is, only part of Fe is reversibly alloyed with Sn during first cycling, and the rest of Fe is inactive. Concluded from the smaller magnitude of the magnetic change, the active metallic Fe decreased gradually.[45]

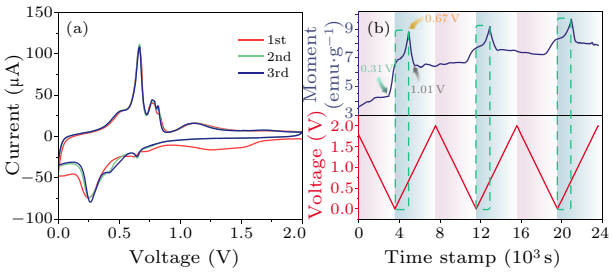

Fig. 2. Reaction mechanism of the Sn_3Fe anode in lithium-ion batteries. (a) Cyclic voltammetry (CV) test of first three cycles with a scan rate of 0.5 mV·s^{-1}. (b) Operando magnetic response of LIBs under an applied magnetic field strength of 1 T conducted during the CV test.

Although the magnetic response of the following two cycles keeps the same trend, it is noteworthy that the overall magnetization is stepwise increase with cycles progress. According to previous reports,[45] this may be due to the fact that Fe nanoparticles produced by lithiation are superparamagnetic and increase in size during the cycling. The Fe nanoparticles produced by the insertion of Li are so small as to show superparamagnetic behavior with magnetization dependent strongly on temperature.[46,47] The formation of Fe nanoparticles was examined by high resolution TEM (HRTEM) of the Sn_3Fe anode discharged to 0 V as visualized in Fig. 3(a). It shows that Fe is approximately a few nanometers in size, and the clear lattice stripe with a spacing of 0.202 nm corresponds to the (110) plane.[48] The rings of selected area electron diffraction (SAED) pattern in Fig. 3(b) can be assigned to the (310), (200) and (110) planes of the Fe phase, which verifies the composition of the nanometer-scale Fe.[49] However, due to the limitation of the detected region, HRTEM can only characterize the local region, and its penetration depth is generally less than 200 nm, thus the information of the entire electrode cannot be obtained.

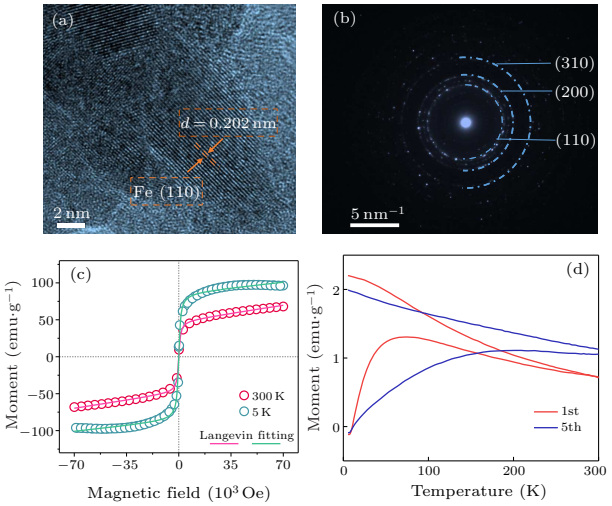

Fig. 3. (a) HRTEM and (b) SAED spectra of Sn_3Fe LIBs discharging to 0.01 V. (c) Hysteresis loop after the first discharge at different temperatures. (d) ZFC/FC curves of Sn–Fe LIBs under different cycles.

In order to further determine this hypothesis that the magnetization increases step by step as the increment in superparamagnetic Fe grains size, it deserves a further exploration of the magnetization as a function of temperature and magnetic field. The magnetic behavior of Sn_3Fe is explored within the initial discharge process to 0 V. In the hysteresis loops of Fig. 3(c), Sn_3Fe LIBs display the expected superparamagnetic characteristics at 300 K, with a magnetization exposition of unsaturation and no coercivity even at a high field of 7 T. Figure 3(c) shows that the fitted curves coincide the experimental curves at 300 K and 5 K, and the diameter of superparamagnetic Fe nanoparticles calculated by Langevin fitting at 300 K is 4.36 nm, which is in great alignment with 4.28 nm calculated at 5 K (Information I in the Supplementary Material). Subsequently, we characterized the magnetization of Sn_3Fe LIBs that discharged to 0 V as a function of temperature (FC and ZFC) in Fig. 3(d). The electrode demonstrates the typical signature of

superparamagnetic particles with a maximum in the ZFC around 65 K and 200 K (blocking temperature, T_B) corresponding to the first and fifth cycles. In accordance with the relationship between the particle diameter d and T_B (Information Ⅱ in the Supplementary Material), the average diameter of Fe nanoparticles can be estimated to be 4.4 nm in the first cycle. A significantly higher T_B in the fifth cycle implies the superparamagnetic nanoparticles with larger size about 6.5 nm, which may be related with the volume expansion during the alloying process.[45] Therefore, through the hysteresis loops and FC/ZFC measurement, we proved that the overall magnetization gradually increased during the cycling was caused by the increasing size of superparamagnetic Fe nanoparticles. Although the inactive Fe produced by the first lithiation process does not participate in the electrochemical reaction, it can improve the electrochemical performance of the batteries as buffer matrix and good electronic conductor.[30] However, excessive aggregated superparamagnetic Fe may form an impenetrable skin on the surface of grains, preventing the adequate transport of Li^+ in intermetallic and resulted in less than excellent performance.[50–52]

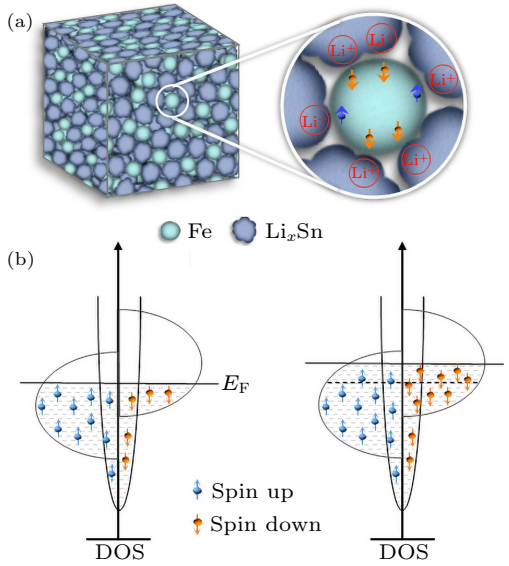

Fig. 4. (a) Interface storage model diagram. (b) Schematic of spin-polarized density of states at the surface of ferromagnetic metal grains before and after electronic filling.

Surprisingly, as shown in the green dotted frame marked in Fig. 2(b), the magnetic responses exhibit an abnormal rise during the charging process from 0 to 0.67 V, which is contrary to the decline of magnetization due to the decrease of iron content. This abnormal magnetic response suggests a space charge storage phenomenon that was recently been magnetically proved.[39] The spin-polarized charges automatically store at the interface of the Fe/Li_xSn heterostructure, that is to say, Li^+ ions are adsorbed on one side of Li_xSn while electrons are injected into adjacent Fe grains [Fig. 4(a)]. The charges accumulated at the Fe nanograins interface will cause the magnetization changes, due to the spin splitting of iron's 3d energy levels [Fig. 4(b)].[53] On account of the net magnetization, closely related to the effective magnetic moment of spin-polarized electrons, the change in the saturation magnetization should be a monotonic reduction during electron filling. Inversely, magnetization increases as electrons dissipate from Fe at the interface, corresponding to the magnetic response in the voltage range of 0–0.67 V during charging. The abnormal magnetic response demonstrated the existence of space charge phenomenon in Sn–Fe alloy, which provides extra capacity.[39,54–56] However, the magnetization decrease caused by the accumulation of electrons on Fe upon lithiation is not observed. This can be attributed to that the signal of a decrease in magnetization caused by space charge phenomenon is offset by the generation of metallic Fe nanoparticles. We excellently proved the existence of space charge effect in Sn–Fe alloy, which provides a path for design of electrode materials with high performance.

In conclusion, high purity Sn–Fe alloy was prepared by magnetron sputtering and its electrochemical mechanism was researched by operando magnetometry. A relatively higher magnetic response after charging than the initial discharge was observed, indicating a partially reversible alloying/dealloying process. Further magnetic measurement showed that the distinctive stepwise rising in magnetization was caused by the larger Fe particles as the number of cycle increase. In addition, we found the mechanism of space charge storage in alloy materials, which provides extra capacity for batteries. These crucial results reveal the role of transition metals in the electrochemical process, and provide a theoretical cornerstone for design of high-performance electrode materials.

Acknowledgements. This work was supported by the National Natural Science Foundation of China (Grant Nos. 22179066 and 11504192), and the Natural Science Foundation of Shandong Province (Grant No. ZR2020MA073).

References

[1] Armand M and Tarascon J M 2008 *Nature* **451** 652
[2] Han Y *et al.* 2020 *Small* **16** 1902841
[3] Barnes D G *et al.* 2013 *PLoS One* **8** e69446
[4] Zhou L M *et al.* 2018 *Adv. Energy Mater.* **8** 1701415
[5] Li W H *et al.* 2020 *J. Energy Chem.* **50** 416
[6] Ouyang C *et al.* 2005 *Chin. Phys. Lett.* **22** 489
[7] Liu Y *et al.* 2021 *Electrochim. Acta* **396** 139265
[8] Zhang L *et al.* 2020 *Adv. Mater.* **32** 1908445
[9] Bruce P G *et al.* 2008 *Angew. Chem. Int. Ed. Engl.* **47** 2930
[10] Goodenough J B and Kim Y 2010 *Chem. Mater.* **22** 587
[11] Park C M *et al.* 2010 *Chem. Soc. Rev.* **39** 3115
[12] Zhao Y *et al.* 2019 *ACS Nano* **13** 5602

[13] Yang S *et al.* 2003 *Electrochem. Commun.* **5** 587
[14] Xin F X *et al.* 2015 *ACS Appl. Mater. Interfaces* **7** 7912
[15] Ying H and Han W Q 2017 *Adv. Sci.* **4** 1700298
[16] Wu X *et al.* 2016 *J. Power Sources* **307** 753
[17] Zhou X *et al.* 2016 *Adv. Energy Mater.* **6** 1601177
[18] Ferrara G *et al.* 2012 *J. Power Sources* **211** 103
[19] Park C and Sohn H 2010 *Electrochim. Acta* **17** 4987
[20] Liang S *et al.* 2020 *Small Methods* **4** 2000218
[21] Nguyen T L *et al.* 2018 *Electrochim. Acta* **278** 25
[22] Shi H *et al.* 2018 *Nano Lett.* **18** 3193
[23] Sony's new nexelion hybrid lithium ion bateries to have thirty-percent more capacity than conventional offering 2005 https://www.sony.com/en/SonyInfo/News/Press/200502/05-006E/
[24] Kim H *et al.* 2020 *Chem. Rev.* **120** 6934
[25] Shen K *et al.* 2019 *Adv. Energy Mater.* **9** 1900260
[26] Lu Y *et al.* 2014 *Nat. Mater.* **13** 961
[27] Chamas M *et al.* 2013 *Chem. Mater.* **25** 2410
[28] Chamas M *et al.* 2011 *Electrochim. Acta* **56** 6732
[29] Dong Z *et al.* 2016 *Adv. Sci.* **3** 1500229
[30] Mao O *et al.* 2019 *J. Electrochem. Soc.* **146** 405
[31] Nwokeke U G *et al.* 2010 *Chem. Mater.* **22** 2268
[32] Dong Z *et al.* 2019 *ACS Omega* **4** 22345
[33] Wu Y and Liu N 2018 *Chem* **4** 438
[34] Jangid M K and Mukhopadhyay A 2019 *J. Mater. Chem. A* **7** 23679
[35] Yang Y *et al.* 2017 *Adv. Mater.* **29** 1606922
[36] Kalantzopoulos G N *et al.* 2018 *ChemPhysChem* **19** 519
[37] Topolovec S *et al.* 2016 *J. Solid State Electrochem.* **20** 1491
[38] Klinser G *et al.* 2016 *Solid State Ionics* **293** 64
[39] Li Q *et al.* 2021 *Nat. Mater.* **20** 76
[40] Wang K *et al.* 2017 *Carbon* **125** 375
[41] Li J T *et al.* 2010 *J. Power Sources* **195** 8251
[42] Li S *et al.* 2020 *Environ. Int.* **138** 105639
[43] Siegel G *et al.* 2015 *Sci. Rep.* **4** 4429
[44] Wang Z *et al.* 2013 *Energy Environ. Sci.* **6** 87
[45] Gershinsky G *et al.* 2014 *Energy Environ. Sci.* **7** 2012
[46] Diandra L L and Rieke R D 1996 *Chem. Mater.* **8** 1770
[47] Huber D L 2005 *Small* **1** 482
[48] Wang F *et al.* 2011 *J. Am. Chem. Soc.* **133** 18828
[49] Zhao L *et al.* 2014 *Adv. Funct. Mater.* **24** 5557
[50] Mao O and Dahna J 1999 *J. Electrochem. Soc.* **146** 414
[51] Li J T *et al.* 2011 *J. Phys. Chem. C* **115** 7012
[52] Ionica-Bousquet C M *et al.* 2006 *Chem. Mater.* **18** 6442
[53] Ouyang C Y *et al.* 2006 *Chin. Phys. Lett.* **23** 61
[54] Zhang F *et al.* 2021 *Matter* **4** 3605
[55] Li H *et al.* 2021 *Adv. Mater.* **33** 2006629
[56] Li Z *et al.* 2021 *J. Am. Chem. Soc.* **143** 12800

Supplementary Material for "Operando Magnetometry Reveals the Electrochemical Role of Transition Metals in Sn-Fe Alloy"

Le-Qing Zhang(张乐清)[1], Qing-Tao Xia(夏清涛)[1], Zhao-Hui Li(李召辉)[1], Yuan-Yuan Han(韩媛媛)[1], Xi-Xiang Xu(徐熙祥)[1], Xin-Long Zhao(赵新龙)[1], Wang Xia(王霞)[1], Yuan-Yuan Pan(潘圆圆)[1], Hong-Sen Li(李洪森)[1] and Qiang Li(李强)[1,2*]

[1]College of Physics, Qingdao University, Qingdao 266071, China
[2]Weihai Innovation Institute, Qingdao University, Weihai 264200, China

*Corresponding author. Email: liqiang@qdu.edu.cn

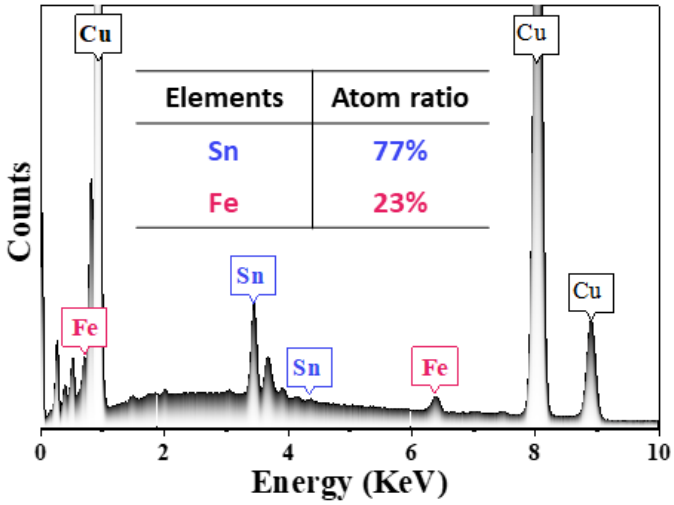

Fig. S1. EDX spectrum of the pristine sample, the Sn and Fe atomic ratios of 77% and 23%, respectively.

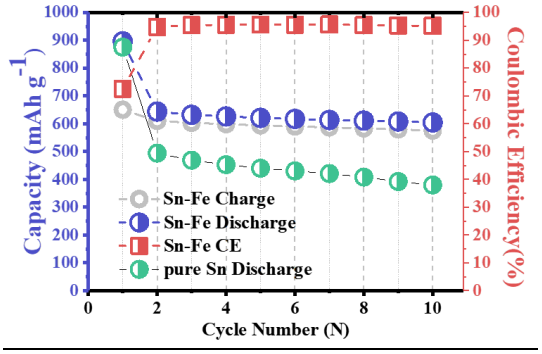

Fig. S2 Cycling performance and coulombic efficiency of Sn_3Fe and pure Sn electrode at 100 mA g^{-1}.

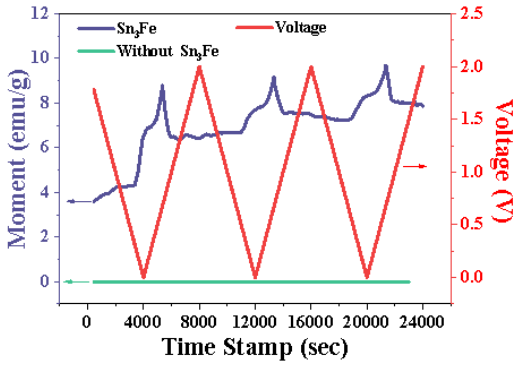

Fig. S3 Comparison of time-sequenced magnetic responses at an applied magnetic field of 3 tesla with respect to CV scans at a scan rate of 0.5 mV s^{-1}.

Information I

Supplementary fitting of superparamagnetic magnetization

The magnetization of superferromagnetic particles can be obtained by Langevin function: $M(H,T) = M_0 L(\mu_p H / kT)$, where M_0 is the saturation magnetization, $L(x) = \coth x - (1/x)$, μ_p is the magnetization of the individual particles. Considering the magnetic moments of each Fe atom are $2.2\,\mu_B$, it is obtained by fitting the experimental curves that the diameter of Fe particles is approximately 4.3 nm.

Supporting Information II

The relationship between the particle diameter d and T_B: $d = (150 k_B T_B / \pi K_{eff})^{1/3}$, where k_B is the Boltzmann constant 1.38×10^{-23} J K^{-1}, T_B is blocking temperature, and K_{eff} is the effective magnetic anisotropy constant. In terms of Fe nanoparticle, K_{eff} is assumed to 4.8×10^5 J m^{-3}. Thus, the approximations of average diameters are 4.4 nm and 6.5 nm corresponding to T_B values of 65 K and 200 K, respectively.